**ORIGINAL ARTICLE**

# Bainite Transformation Behavior and Mechanical Characteristics of Medium-Carbon High-Silicon Steel via Austempering

Xiaolin Wang[1,2] · Qixiang Xu[1,2] · Zhaojun Fu[3] ·
Qiang Li[1,2] · Hui Guo[1,2]

**Abstract** A series of austempering processes above and below the martensite start temperature (Ms) were employed to evaluate the effect of various austempering temperatures on bainite transformation kinetics, microstructural characterization and mechanical properties of medium-carbon high-silicon steel. The results demonstrated that lowering austempering temperature from above Ms to below Ms brought about the increase of prior martensite content, the refinement of bainitic ferrite lath and the reduction of blocky retained austenite amount and size, which simultaneously accelerated the bainite transformation kinetics and improved the tensile strength as well as impact toughness. Unfortunately, decreasing the austempering temperature reduced the retained austenite content and, thus, led to a marginal drop in elongation. By an integrated consideration of phase transformation kinetics and mechanical performance, the austempering process below and close to the Ms temperature would impart outstanding overall mechanical properties.

**Keywords** Austempering · Martensite start temperature · Phase transformation kinetics · Mechanical properties

✉ Hui Guo
   guohuiyw@126.com

1   University Featured Laboratory of Materials Engineering for Agricultural Machinery of Shandong Province, Weifang University of Science and Technology, Weifang 262700, China

2   Weifang Key Lab of Advanced Light Materials Manufacturing and Forming, Weifang University of Science and Technology, Weifang 262700, China

3   Shandong Haihua Energy Co., Ltd, Weifang 262700, China

## 1 Introduction

For the sake of fulfilling the simultaneous requirement of decreasing component weight to improve energy efficiency and safety, the development and application of advanced high-strength steel in the automotive industry appear to be particularly important. Due to its ultrahigh strength combined with adequate ductility, ultrafine bainitic steel presents a promising candidate for producing energy-efficient components and has received considerable attention [1–3]. In general, the multiphase microstructure of ultrafine bainitic steel, consisting primarily of bainitic ferrite and retained austenite, can be achieved by simple austempering procedures without adding a high proportion of alloy elements. The extraordinarily slender bainitic ferrite lath with high dislocation density ensures the ultrahigh strength, while the presence of sufficient retained austenite content accompanied with adequate carbon concentration provides the excellent ductility by the transformation-induced plasticity (TRIP) effect [4–6].

In recent years, a large number of studies have been undertaken on various austempering treatments to tune the transformation kinetics, resultant microstructure and mechanical properties [7–12]. Navarro–López et al. [8] succeed in modeling the overall mechanical response of a low-carbon high-silicon steel based on grain-boundary, solid solution and precipitation strengthening in the presence of prior martensite, to reveal the improved mechanical properties compared to specimens treated with conventional treatments above Ms. The strengthening model of bainitic multiphase steel involving the correlation between yield strength and phase fractions/phase constituents was also established by Sun et al. [9]. Yao et al. [10] reported that the size and content of blocky retained austenite would be reduced by the formation of prior martensite as the austempering temperature decreased from above to below Ms, thus

improving the tensile strength and impact toughness. It has been demonstrated that the optimal TRIP effect and relatively uniform strain partitioning between different phases drastically affected the mechanical performance of ultrafine bainitic steel in the existence of prior martensite [11, 12]. Long et al. [13] also suggested that the benefit of excellent work hardening ability and improved plasticity toughness of below-Ms process came from the increased volume fraction and mechanical stability of retained austenite. However, some discordant results reported that the below-Ms austempering process did greatly bring about the resultant microstructure refinement of low-carbon bainitic steel, yet resulted in a decrease in yield strength as well as the product of tensile strength and elongation [14]. The previously contradictory results described in the literature mainly resulted from the different alloy compositions and phase constituents, especially the presence of fresh martensite. Therefore, more studies should be required to further understand whether the different austempering temperatures have a positive or negative effect on bainite transformation, under the rational composition design and microstructure regulation.

In this work, the bainite transformation kinetics, microstructural characterization and mechanical properties of ultrafine bainitic steel subjected to austempering treatments below or above Ms were systematically evaluated. These results held important implications for tuning the processing parameters to manufacture various industrial products.

## 2 Materials and Methods

The steel used in the present work was melted in a vacuum induction furnace with a nominal composition of Fe-0.3C-2.0Si-1.5Mn-2.0Cr-1.0Ni (wt%). A 50-kg cast ingot was forged into square billets with dimensions of 150 mm × 70 mm × 70 mm and homogenized at 1200 °C for 24 h, followed by hot rolling to a thickness of 12 mm

at a finishing temperature of 950 °C. Thermal simulation experiments were performed to determine the phase transformation temperatures and to quantitatively evaluate the bainite transformation kinetics, using a DIL 805A dilatometer on cylindrical specimens with a diameter of 4 mm and a length of 10 mm. The $Ac_1$, $Ac_3$ and Ms were determined to be approximately 760, 870 and 310 °C, respectively, as illustrated schematically in Fig. 1a. According to the processing schedules revealed in Fig. 1b, the samples were austenitized at 950 °C for 20 min followed by isothermal holding at 330, 320, 300 and 290 °C for 1 h, respectively, and then cooled to room temperature. For simplicity, the specimens isothermally held at 290, 300, 320 and 330 °C were hereafter termed as the below-Ms (290 and 300 °C) and above-Ms specimens (320 and 330 °C), respectively.

The uniaxial tensile samples with a gage diameter of 5 mm and a gage length of 25 mm were taken from the hot-rolled slabs along the rolling direction. The quasi-tensile tests were performed on a 100 kN MTS 810 tensile testing machine at a constant cross-head velocity of 1 mm/min. The yield strength was defined by the 0.2% offset method. Impact tests were conducted on the Charpy V-notch sample with a dimension of 10 mm × 10 mm × 55 mm using an impact testing machine at room temperature. Bulk hardness measurements were taken using a micro-Vickers hardness tester with a dead load of 10 kgf. Ten different measurements per condition were taken to confirm reproducibility.

X-ray diffraction (XRD) analysis was performed using a Bruker D8 Advance diffractometer equipped with a Cu Kα radiation operating at 40 kV. The scanning range was in the range of 47°-93°, and the scanning rate was 1°/min with a counting time per step of 2 s. The volume fraction of retained austenite was determined quantitatively from the integrated intensities of $(200)_\gamma$, $(220)_\gamma$, $(311)_\gamma$ and $(200)_\alpha$, $(211)_\alpha$ diffraction peaks according to the direct comparison method [15].
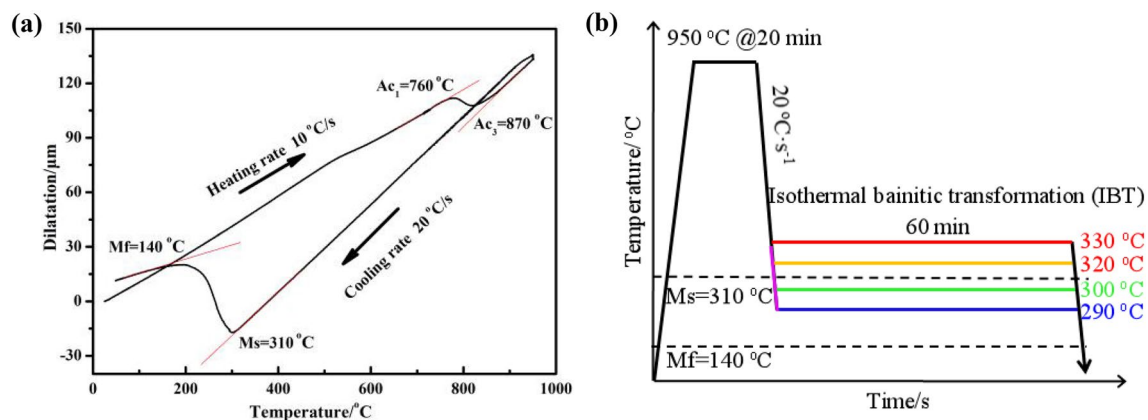


**Fig. 1** **a** Phase transformation temperatures determined by dilatometer, **b** schematic diagram of heat treatment routes

The microstructure observation and fracture surface morphology of impact samples were carried out on a scanning electron microscope (SEM). Samples for microstructural examination were prepared by standard metallographic procedures of mechanical grinding, polishing and etching in 4% Nital solution. Transmission electron microscope (TEM) was employed to detect different phases and to evaluate the average thickness of bainite lath. A more detailed TEM experimental procedure can be found elsewhere [16]. The true scale of bainitic ferrite lath was determined and corrected using the method proposed in the literature [17].

## 3 Results and Discussion

The relative changes in length of dilatometry samples as a function of temperature during isothermal holding and cooling to room temperature are shown in Fig. 2a. Evidently, no deviation point from linearity can be detected in the dilatometry curves during final cooling to room temperature after isothermal treatment except the specimen austempered at 330 °C, as indicated by the dashed square box. The deviation in dilatation-temperature curve represents the formation of fresh martensite. As the holding temperature decreases to 300 or 290 °C, the different volume fractions of prior martensite (PM) are produced, as confirmed by the apparent inflection point at 310 °C. The length increment with ongoing isothermal holding reflects the continuous formation of isothermal product, previously confirmed by Samanta et al. [18] as bainitic ferrite. The larger expansion corresponds to the higher content of formed bainite. Accordingly, after the identical holding duration, the specimen austempered at 320 °C appears to contain a higher volume fraction of bainitic ferrite.

The length changes of dilatometry samples against transformation time during isothermal holding at different temperatures are exhibited in Fig. 2b. As is evident from the curves that the bainite transformation kinetics of above-Ms specimens follow an S-shape, and the incubation time of bainite transformation is slightly shortened with increasing transformation temperature for above-Ms specimens, but the total completion time does not differ so much. However, for below-Ms specimens, an initial rapid rise can be seen in the curve, rather than in the S-shape. More importantly, the bainite transformation initiates with a significantly shorter incubation period, followed by a steeper expansion and a considerably shorter completion time than the above-Ms specimens. This phenomenon indicates that the introduction of prior martensite can exert a significantly positive effect on bainite formation kinetics at the early stage of isothermal transformation and strongly accelerate the subsequent bainite transformation. In addition, the improvement in transformation kinetics comes not only from the additional bainitic subunits nucleation sites provided by the presence of prior martensite boundaries, but also from the higher total driving energy of bainite formation resulting from the lower austempering temperature [19–21].

The SEM micrographs of the specimens after isothermal holding at various temperatures are displayed in Fig. 3. Distinctly, the main transformation products of above-Ms specimens consist primarily of bainite in the form of lath and martensite/austenite (M/A) island being dominant by irregular morphology (Figs. 3a and b), and the alignment of bainite lath within an austenite grain can be at random angles. Unsatisfactorily, it is rather tricky to differentiate fresh martensite and retained austenite from SEM micrographs. One can clearly see that the size and proportion of M/A island gradually reduce with decreasing holding temperature. Statistical results show that the mean size of M/A island reduces from $3.2 \pm 0.2$ to $2.3 \pm 0.3$ μm with decreasing isothermal temperature from 330 to 320 °C.
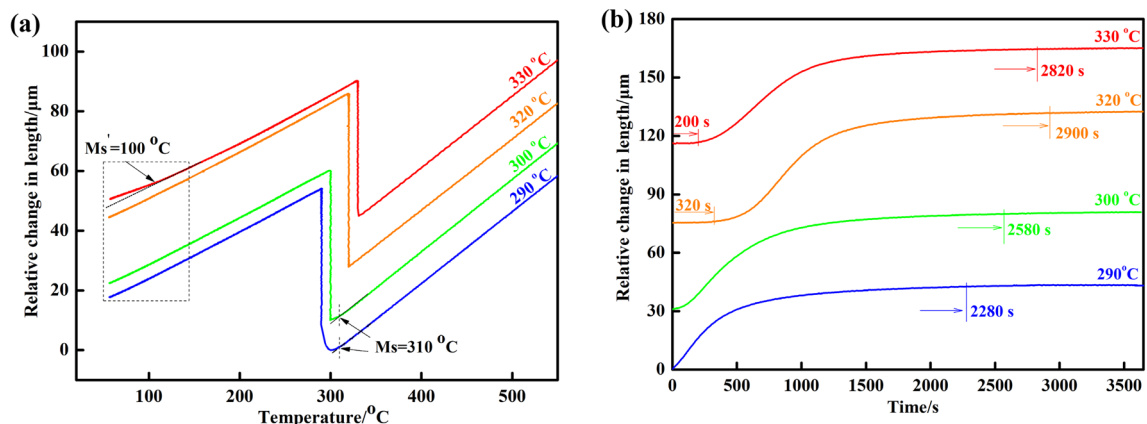


**Fig. 2** Relative change in length as a function of, **a** temperature and **b** time obtained from dilatometry
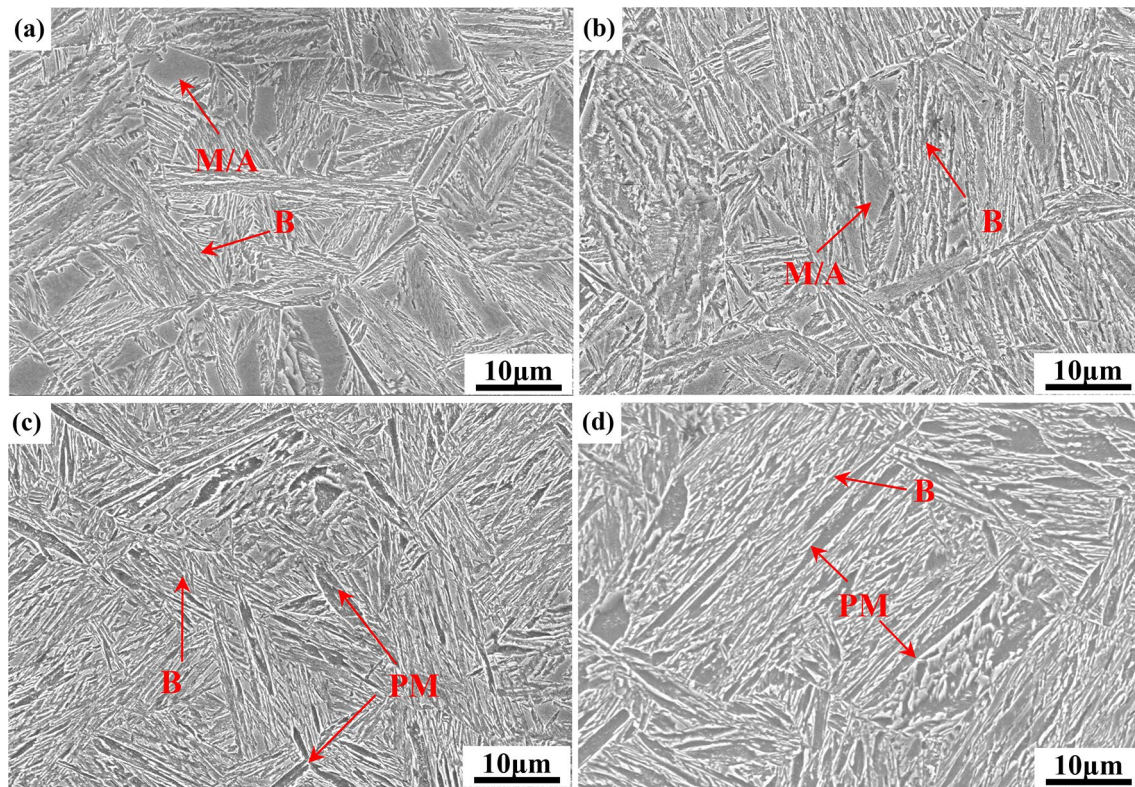
**Fig. 3** SEM micrographs of the specimens subjected to isothermal holding at, **a** 330 °C, **b** 320 °C, **c** 300 °C and **d** 290 °C. Where M/A, B and PM refer to martensite/austenite island, bainite and prior martensite, respectively

Nevertheless, the below-Ms specimens contain a mixture of bainite sheaves and prior martensite, with almost undetectable M/A island in the microstructure (Fig. 3c and d). Meanwhile, no distinctive differences can be observed within the microstructure, except for the increase of prior martensite content with decreasing isothermal temperature. The refinement or elimination of blocky retained austenite can be attributed to two reasons. On the one hand, the PM can refine blocky retained austenite and bainite sheaves by dividing the prior austenite grain into several parts. On the other hand, the increased nucleation site by incorporating a small amount of PM makes a contribution to the increase of bainitic subunits, which brings about the reduction of size and amount of blocky retained austenite distributed between different orientations of bainitic sheaves.

The TEM micrographs of the specimens subjected to various temperatures are shown in Fig. 4. All bainitic sheaves consist mainly of bainitic ferrite lath and filmy retained austenite located between them, irrespective of above-Ms and below-Ms specimens. Apparently, the average thicknesses of bainitic ferrite and filmy retained austenite are gradually refined with decreasing holding temperature. Moreover, the retained austenite in above-Ms specimens takes on two forms of morphologies as follows, film-like appearance and polygonal shape in two-dimensional sections. Meanwhile,

the blocky retained austenite in the specimen austempered at 330 and 320 °C can be easily distinguished by the selected area electron diffraction patterns shown in Figs. 4a and b.

Additionally, the microstructures of below-Ms specimens are decorated by prior martensite instead of irregular-shaped M/A islands, as shown in Fig. 4c and d. Further analysis by TEM declares that carbides can be clearly identified in the prior martensite due to tempering to some extent in the process of isothermal treatment. The refined microstructure obtained by below-Ms austempering process is primarily correlated with two mechanisms. Firstly, the lower austempering temperature corresponds to the larger degree of undercooling, thus increasing the free energy available for bainite transformation. Another reason is that the additional interface existing between the prior martensite provides more nucleation sites for bainitic subunits, which gives rise to the refinement of bainitic ferrite.

The XRD spectra of samples subjected to different isothermal heat treatments are illustrated in Fig. 5a, which reveals that only two kinds of diffraction peaks can be identified, namely BCC peaks referring to bainite and martensite and FCC peaks to retained austenite. Obviously, the intensity of retained austenite diffraction peak gradually reduces with decreasing transformation temperature, indicating the minimized volume fraction of retained austenite.
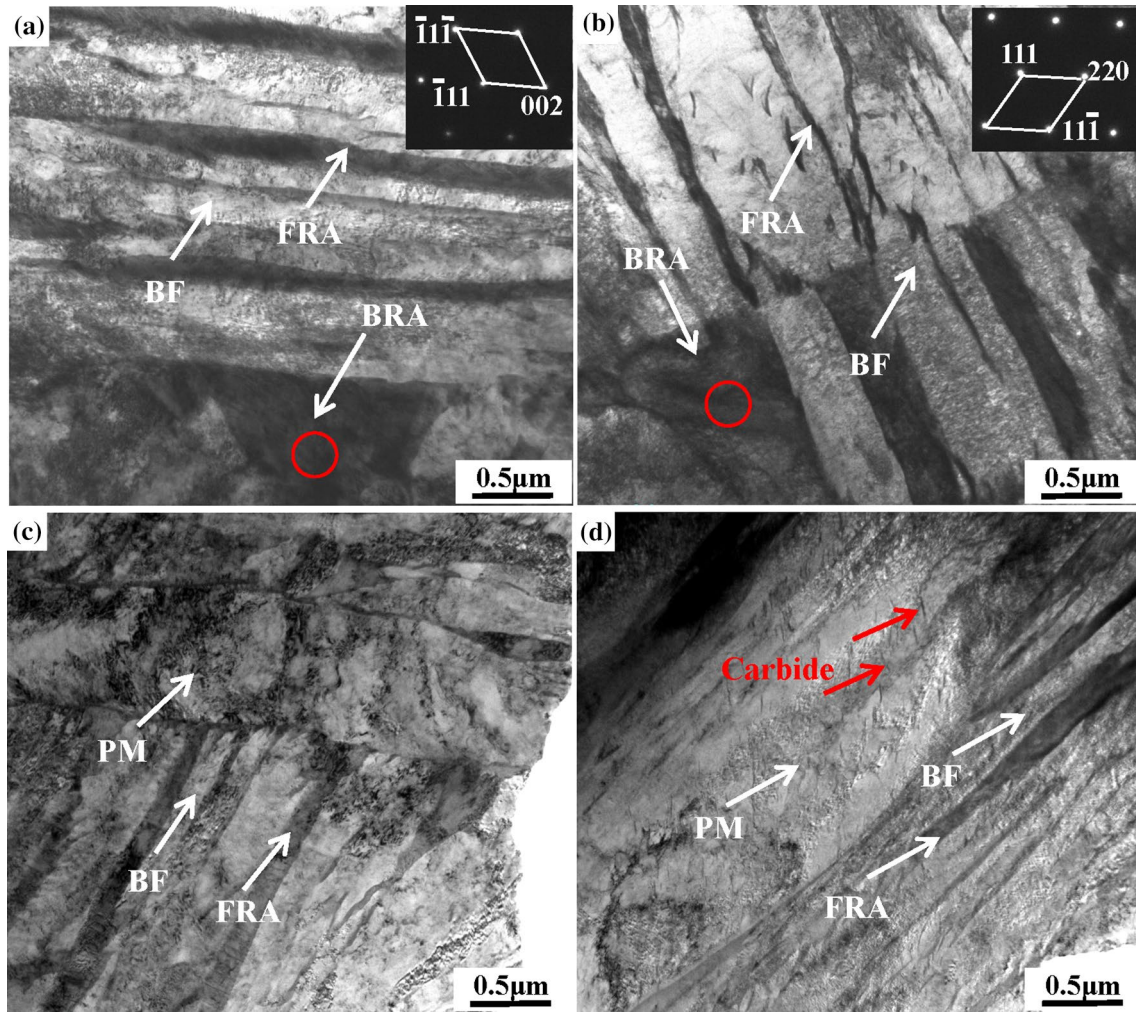
**Fig. 4** TEM micrographs of the specimens subjected to isothermal holding at, **a** 330 °C, **b** 320 °C, **c** 300 °C and **d** 290 °C. Where BRA, BF, FRA and PM refer to blocky retained austenite, bainitic ferrite, filmy retained austenite and prior martensite, respectively
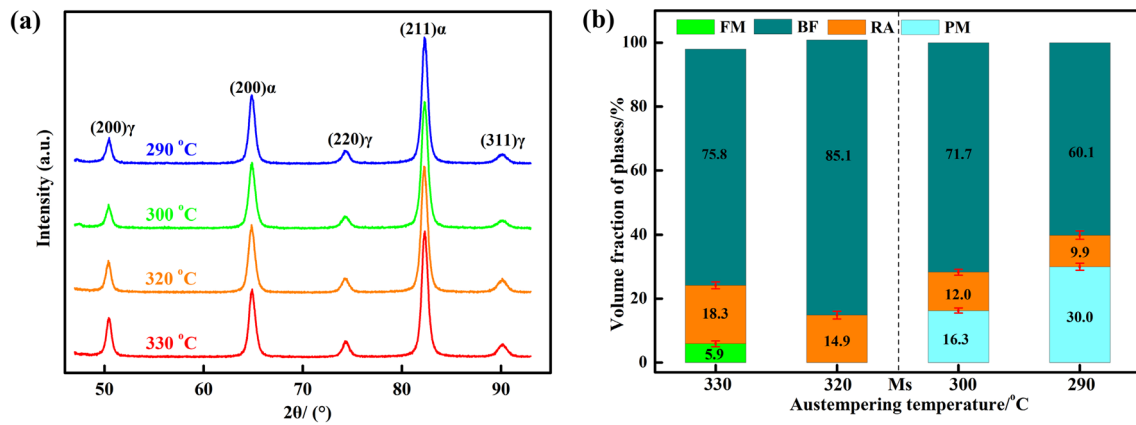


**Fig. 5 a** XRD spectra of samples subjected to different isothermal heat treatments, **b** volume fraction of various phases. Where FM, BF, RA and PM stand for fresh martensite, bainitic ferrite, retained austenite and prior martensite

Quantitative calculation of the constituent phases is of great importance to gain a comprehensive understanding of phase transformation. For above-Ms process, the sufficiently unstable undercooled austenite in the specimen austempered at 330 °C readily experiences a transformation to martensite upon quenching after isothermal bainite transformation. The Ms' temperature of remaining untransformed austenite after termination of isothermally transformed bainite is measured as approximately 100 °C. Therefore, assuming that only carbon partitioning from the created bainitic ferrite to the surrounding austenite takes place during the progression of isothermal transformation, while the alloy element content can be equal to the nominal composition. Thus, the carbon concentration of austenite ($x_C$) after isothermal treatment can be estimated using established empirical Eq. 1 [22].

$$x_C = \left( \frac{692 - 37*x_{Mn} - 14*x_{Si} - 11*x_{Cr} - M_s'}{502} \right)^2 \quad (1)$$

where the $x_i$ stands for the alloy element content in wt.%, Ms' for the measured martensite transformation temperature of survived austenite.

Correspondingly, the experimental volume fraction of freshly formed martensite ($f_M$) at a given temperature can be calculated by using the Koistinen and Marburger (KM) model, which has been used to best distinguish the decomposition of undercooled austenite into martensite [23].

$$f_M = 1 - \exp(-\alpha_m(T_{Ms} - T)) \quad (2)$$

where $T$ stands for the quenching temperature, $T_{Ms}$ for the theoretical martensite transformation temperature of survived austenite that is M'$_s$, $\alpha_m$ stands for the rate parameter which can be calculated by the following equation [24].

$$\alpha_m = 0.0224 - 0.0107x_c - 0.0007x_{Mn} - 0.00005x_{Ni} - 0.00012x_{Cr} \quad (3)$$

Then, the volume fraction of bainitic ferrite ($f_{BF}$) can be expressed by the formula:

$$f_{BF} = 1 - f_{RA} - f_{M*}(1 - f_{BF}) \quad (4)$$

where $f_{RA}$ stands for the calculated RA by XRD.

In contrast, for isothermal treatments below-Ms, some of primary austenite initially decomposes into PM as soon as the temperature is cooled below Ms, as supported by the dilatometric curves, and then the rest of austenite transforms into bainite in the subsequent isothermal holding process. For the specimens austempered at 290 and 300 °C, the volume fraction of PM transformed from austenite is, respectively, calculated to be approximately 16.3% and 30.0% by the K–M model, as expressed in Eq. 2. Finally, it gives the formed bainitic ferrite as a remnant.

The fraction of each phase measured by the above method is displayed in Fig. 5b. It can be discerned that the bainite content initially increases with a decrease in transformation temperature, reaching a maximum value of 85.1% at 320 °C, and then continuously minimizes until it reaches a minimum level of 60.1% at 290 °C.

The engineering stress–strain curves of the specimens subjected to various isothermal temperatures are shown in Fig. 6a. It is readily apparent that all stress–strain curves exhibit continuous yielding behavior, which is similar to that of dual-phase steel. This phenomenon is associated with the presence of high-density movable dislocations introduced by the displacive growth of bainitic ferrite [25]. It is clearly demonstrated that the yield strength (YS) and ultimate tensile strength (UTS) increase from 790 to 1080 MPa and 1410 MPa to 1650 MPa, respectively, with decreasing temperature from 330 to 290 °C, while the uniform elongation (UE) and total elongation (TE) decrease monotonically, as illustrated in Fig. 6b. That is, the below-Ms specimens perform significantly superior yield and tensile strengths,
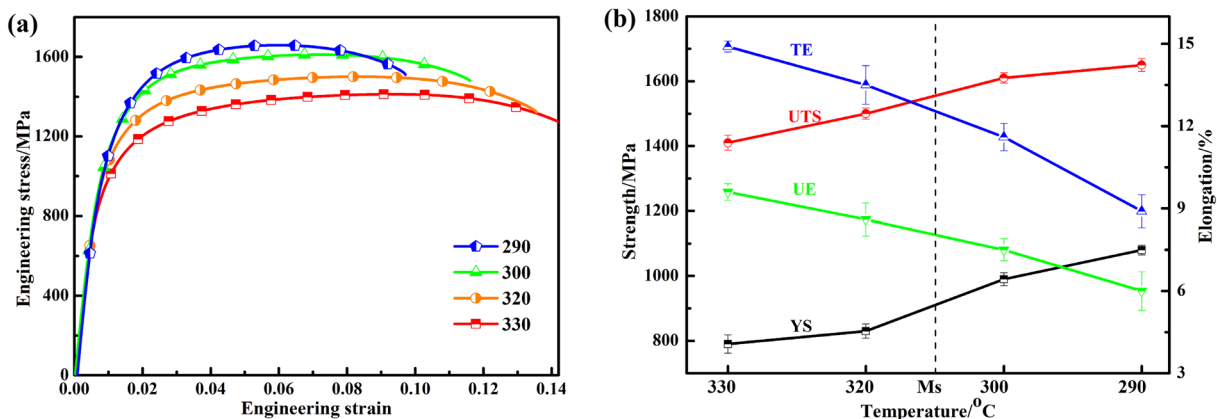


**Fig. 6 a** Engineering stress–strain curves and **b** yield strength (YS), ultimate tensile strength (UTS), uniform elongation (UE) and total elongation (TE) of samples after being subjected to isothermal heat treatment

but somewhat worse ductility, compared to above-Ms specimens. The enhanced strength stems primarily from the refined microstructure of below-Ms specimens, as confirmed by SEM and TEM analysis. The declined ductility with decreasing transformation temperature may be closely related to the lessened retained austenite content and the insufficient TRIP effect [26]. The long-term work hardening behavior being present in the above-Ms specimens is thought to originate mainly from the presence of more blocky retained austenite.

As concluded in previous studies, the blocky retained austenite generally contains a relatively lower carbon concentration and thus succumbs to undergoing strain-induced transformation in the whole stage of deformation, contributing to an improvement in plastic strain [26, 27]. Conversely in below-Ms processes, the more filmy retained austenite having sufficient stability remains even stable throughout the course of deformation, which results in the relatively lower ductility.

The hardness and impact toughness of samples after various austempering processes are depicted in Fig. 7. As the austempering temperature declines, the hardness exhibits an almost linear increasing trend, which mainly ascribes to the refined microstructure and the increased hardness of martensite phase as relative to bainite phase. However, the impact toughness initially increases and then descends slightly with decreasing austempering temperature. It has been previously reported that impact toughness is to a large extent related to the morphology and content of retained austenite [27]. Impact toughness can be improved by decreasing the amount and size of austenite blocks as well as replacing austenite blocks with films [27–29], while the microstructure refinement, especially the refined bainitic ferrite lath, will be beneficial in improving crack arrest capability [30, 31]. As a
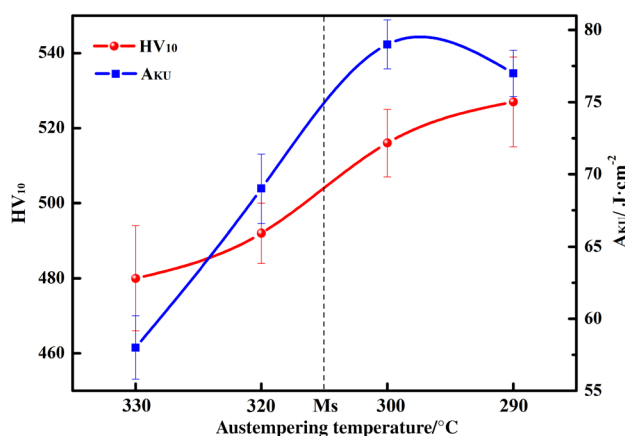
consequence, the below-Ms specimens, which have more volume fraction of filmy retained austenite and refined bainitic ferrite lath, exhibit higher impact toughness compared to above-Ms specimens. More specially, in comparison with 330 °C specimen, the impact toughness of specimen austempered at 300 °C increases by about 36%. In the course of impact deformation, the transformation from filmy retained austenite to martensite taking place at the tip of crack can effectively make crack tip blunting, stress relief and crack closure ahead of the microcrack, which is more conducive to improving the material toughness [32, 33]. However, the impact toughness of below-Ms specimens slightly declines when the austempering temperature reduces to 290 °C. This phenomenon can be partially rationalized considering the decreased amount of retained austenite in the specimen austempered at 290 °C.

The typical SEM micrographs of impact samples after various austempering treatments are demonstrated in Fig. 8. Evidently, the fracture surfaces of below-Ms specimens are predominantly decorated by a small amount of cleavage facets and a large number of tearing edges and dimples, indicating a mixed crack propagation mode of ductile and brittle fracture. With increasing austempering temperature, the number of dimples gradually increases, while the size and amount of cleavage facets simultaneously vary in the opposite trend, exhibiting a significant ductile fracture model. The change in the impact fracture mechanism with increasing austempering temperature may be associated with the diverse microstructural variations and corresponding sizes [34–36]. For above-Ms specimens, the significant fraction of deformation-induced martensite generated from the lower mechanical stability of blocky retained austenite and a small quantity of individual fresh martensite can trigger crack initiation and propagation, which inevitably performs a detrimental effect on impact behavior [28]. Therefore, the quasi-cleavage brittle fracture dominates the impact fracture mechanism in above-Ms specimens. In contrast, numerous dimples and tearing edges are prevalent on the fracture surface of below-Ms specimens, revealing that the typical ductile fracture characteristic appears to be dominant. It is predominantly ascribed to the refined bainitic sheaves and the increased content of filmy retained austenite achieved by below-Ms austempering treatment.

From all the presented results, it seems reasonable to conclude that the incorporation of prior martensite by below-Ms isothermal treatment leads to an improvement in tensile strength and impact toughness, while the above-Ms processes are favorable for enhancing ductility. Consequently, different heat treatment cycles can be designed to tune the microstructural characteristics to achieve the required mechanical properties of medium-carbon high-silicon ultrafine bainitic steel.
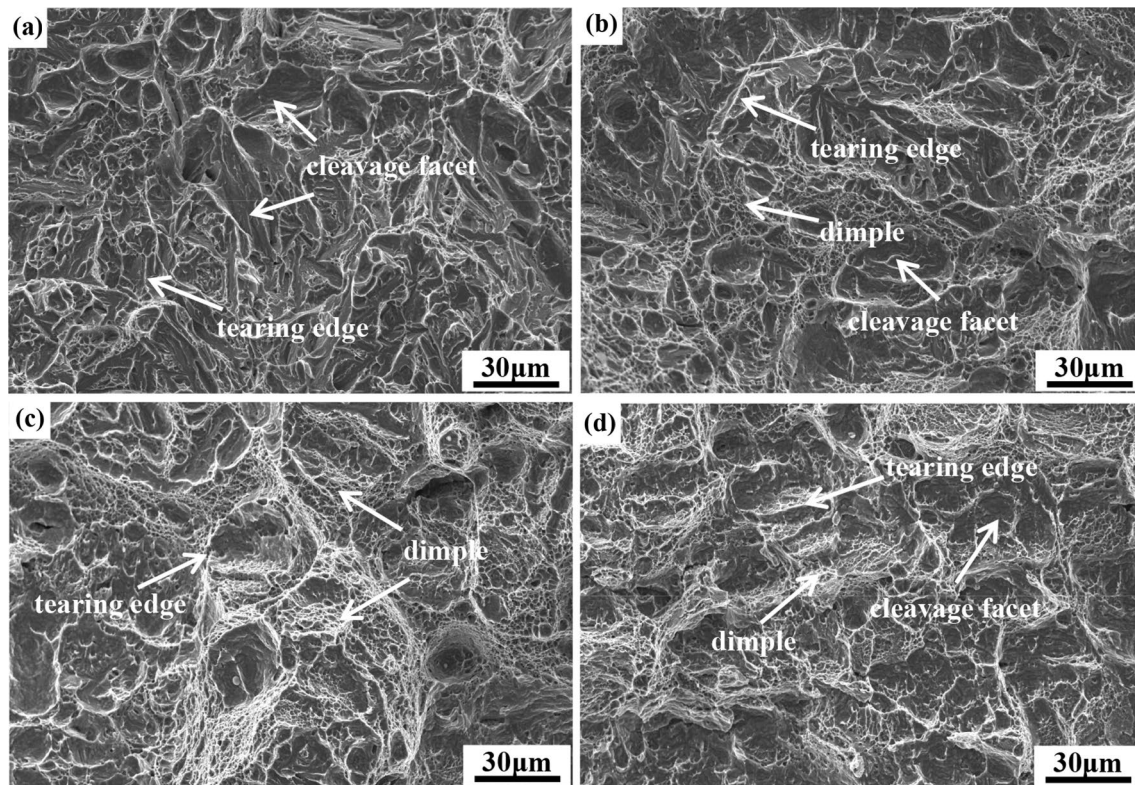


**Fig. 7** Hardness and impact toughness of samples after subjecting to isothermal heat treatment

**Fig. 8** SEM micrographs of impact fracture surface of specimens austempered at, **a** 330 °C, **b** 320 °C, **c** 300 °C and **d** 290 °C

## 4 Conclusion

In this work, the effect of austempering temperatures on the formation of bainitic ferrite and mechanical properties of ultrafine bainitic steel has been qualitatively and quantitatively evaluated by dilatometric experiments, tensile and impact tests. The main conclusions drawn from the present work are as follows.

The prior martensite introduced by below-Ms process tends to shorten bainite incubation period and phase transformation completion time, which exerts a significantly positive effect on bainite formation kinetics.

The below-Ms process effectively reduces the thickness of bainitic ferrite plate, size and amount of blocky retained austenite, thus improving the tensile strength and impact toughness compared to above-Ms process. However, the latter which contains more retained austenite phase exhibits the better performance with respect to ductility.

From the aspect of phase transformation kinetics and mechanical performance, the austempering process below and close to the Ms temperature will be more preferable, which can yield ultimate strength levels beyond 1400 MPa simultaneously with appropriate ductility.

**Declarations**

**Conflict of interest** The authors declare that they have no known competing financial interests or personal relationships that could have appeared to influence the work reported in this paper.

## References

1. Garcia-Mateo C, Caballero F G, and Bhadeshia H K D H, *ISIJ Int.* **43** (2003) 1238. https://doi.org/10.2355/isijinternational.43.1238
2. Zhang F C, and Yang Z N, *Engineering* **5** (2019) 319. https://doi.org/10.1016/j.eng.2018.11.024
3. Hasan S M, Chakrabarti D, and Singh S B, *Wear* **408** (2018) 151. https://doi.org/10.1016/j.wear.2018.05.006
4. García-Mateo C, and Caballero F G, *Mater. Trans.* **46** (2005) 1839. https://doi.org/10.2320/matertrans.46.1839
5. Morales-Rivas L, Yen H W, Huang B W, Kuntz M, Caballero F G, Yang J R, and Garcia-Mateo C, *JOM* **67** (2015) 2223. https://doi.org/10.1007/s11837-015-1562-x
6. Zhao F Y, Chen P, Xu B Y, Yu Q, Misra R D K, Wang G D, and Yi H L, *Mater. Charact.* **179** (2021) 111327. https://doi.org/10.1016/j.matchar.2021.111327
7. Mondal J, Das K, and Das S, *Mater. Charact.* **177** (2021) 111166. https://doi.org/10.1016/j.matchar.2021.111166

8. Navarro-López A, Hidalgo J, Sietsma J, and Santofimia M J, *Mater. Sci. Eng. A* **735** (2018) 343. https://doi.org/10.1016/j.msea.2018.08.047

9. Sun X W, Sun D Y, Wang Y F, Zhang F C, Sheng G L, He Y M, and Wang T S, *J. Mater. Sci.* **57** (2022) 17462. https://doi.org/10.1007/s10853-022-07712-9

10. Yao C X, Lan H F, Tao Z, Misra R D K, and Du L X, *Steel Res. Int.* **92** (2021) 2100263. https://doi.org/10.1002/srin.202100263

11. Zhao L J, Qian L H, Meng J Y, Zhou Q, and Zhang F C, *Scripta Mater.* **112** (2016) 96. https://doi.org/10.1016/j.scriptamat.2015.09.022

12. Qian L H, Li Z, Wang T L, Li D D, Zhang F C, and Meng J Y, *J. Mater. Sci. Technol.* **96** (2022) 69. https://doi.org/10.1016/j.jmst.2021.05.002

13. Long X Y, Sun D T, Wang K, Zhang F C, Yang Z N, Li Y G, and Zheng C L, *J. Mater. Res. Technol.* **17** (2022) 898. https://doi.org/10.1016/j.jmrt.2021.12.121

14. Tian J Y, Xu G, Zhou M X, and Hu H J, *Steel Res. Int.* **89** (2018) 1700469. https://doi.org/10.1002/srin.201700469

15. Sun J, and Yu H, *Mater. Sci. Eng. A* **586** (2013) 100. https://doi.org/10.1016/j.msea.2013.08.021

16. Guo H, Zhao A M, Zhi C, Ding R, and Wang J X, *Mater. Sci. Technol.* **33** (2017) 893. https://doi.org/10.1080/02670836.2016.1245239

17. Chang L C, and Bhadeshia H K D H, *Mater. Sci. Technol.* **11** (1995) 874. https://doi.org/10.1179/026708395790165462

18. Samanta S, Biswas P, Giri S, Singh S B, and Kundu S, *Acta Mater.* **105** (2016) 390. https://doi.org/10.1016/j.actamat.2015.12.027

19. Navarro-López A, Sietsma J, and Santofimia M J, *Metall. Mater. Trans. A* **47** (2016) 1028. https://doi.org/10.1007/s11661-015-3285-6

20. Tian J Y, Xu G, Hu H J, Wand X, and Zurob H, *J. Mater. Res. Technol.* **9** (2020) 13594. https://doi.org/10.1016/j.jmrt.2020.09.119

21. Guo H, Li Q, Su J M, and Feng X Y, *Steel Res. Int.* **92** (2021) 2000708. https://doi.org/10.1002/srin.202000708

22. Kaar S, Steineder K, Schneider R, Krizan D, and Sommitsch C, *Scripta Mater.* **200** (2021) 113923. https://doi.org/10.1016/j.scriptamat.2021.113923

23. Koıstinen D P, and Marbürger R E, *Acta Metall.* **7** (1959) 59. https://doi.org/10.1016/0001-6160(59)90170-1

24. Bohemen S M C, *Mater. Sci. Technol.* **28** (2012) 487. https://doi.org/10.1179/1743284711Y.0000000097

25. Li R T, Zuo X R, Hu Y Y, Wang Z W, and Hu D X, *Mater. Charact.* **62** (2011) 801. https://doi.org/10.1016/j.matchar.2011.05.013

26. Avishan B, *Int. J. Miner. Metall. Mater.* **24** (2017) 1010. https://doi.org/10.1007/s12613-017-1490-6

27. Garbarz B, and Niżnik-Harańczyk B, *Mater. Sci. Technol.* **31** (2015) 773. https://doi.org/10.1179/1743284714Y.0000000675

28. Xia S L, Zhang F C, and Yang Z N, *Mater. Sci. Eng. A* **724** (2018) 103. https://doi.org/10.1016/j.msea.2018.03.067

29. Dong X X, and Shen Y F, *Mater. Sci. Eng. A* **852** (2022) 143737. https://doi.org/10.1016/j.msea.2022.143737

30. Wang T S, Yang J, Shang C J, Li X Y, Zhang B, and Zhang F C, *Scripta Mater.* **61** (2009) 434. https://doi.org/10.1016/j.scriptamat.2009.04.038

31. Wang K, Hu F, Zhou S B, Isayev O, Yershov S, Zhang Y C, and Wu K M, *Mater. Lett.* **324** (2022) 132517. https://doi.org/10.1016/j.matlet.2022.132517

32. Zhou S B, Hu F, Zhou W, Cheng L, Hu C Y, and Wu K M, *J. Mater. Res. Technol.* **14** (2021) 1021. https://doi.org/10.1016/j.jmrt.2021.07.011

33. Fielding L, Jones N G, Walsh J, Boxel S V, Blackmur M S, Lee P D, Withers P J, Stone H J, and Bhadeshia H K D H, *Acta Mater.* **105** (2016) 52. https://doi.org/10.1016/j.actamat.2015.11.029

34. Guo H, Feng X Y, Zhao A M, Li Q, and Chai M J, *J. Mater. Res. Technol.* **9** (2020) 1593. https://doi.org/10.1016/j.jmrt.2019.11.085

35. Kumar A, and Singh A, *Mater. Sci. Eng. A* **729** (2018) 439. https://doi.org/10.1016/j.msea.2018.05.106

36. Lee S I, Lee J M, Kim S G, Song Y B, Kim H K, Shim J H, and Hwang B, *Mater. Sci. Eng. A* **848** (2022) 143334. https://doi.org/10.1016/j.msea.2022.143334